The Astronomical Journal, 141:59 (12pp), 2011 February doi:10.1088/0004-6256/141/2/59

THE REFLECTION EFFECT IN INTERACTING BINARIES OR IN PLANET–STAR SYSTEMS

J. Budaj
Astronomical Institute, Slovak Academy of Sciences, Tatranská Lomnica 05960, Slovak Republic; budaj@ta3.sk
Received 2010 May 20; accepted 2010 November 22; published 2011 January 13

ABSTRACT

There are many similarities between interacting binary stars and stars with a close-in giant extrasolar planet. The reflection effect is a well-known example. Although the generally accepted treatment of this effect in interacting binaries is successful in fitting light curves of eclipsing binaries, it is not very suitable for studying cold objects irradiated by hot objects or extrasolar planets. The aim of this paper is to develop a model of the reflection effect which could be easily incorporated into the present codes for modeling of interacting binaries so that these can be used to study the aforementioned objects. Our model of the reflection effect takes into account the reflection (scattering), heating, and heat redistribution over the surface of the irradiated object. The shape of the object is described by the non-spherical Roche potential expected for close objects. Limb and gravity darkening are included in the calculations of the light output from the system. The model also accounts for the orbital revolution and rotation of the exoplanet with appropriate Doppler shifts for the scattered and thermal radiation. Subsequently, light curves and/or spectra of several exoplanets have been modeled and the effects of the heat redistribution, limb darkening/brightening, (non-)gray albedo, and non-spherical shape have been studied. Recent observations of planet-to-star flux ratio of HD189733b, WASP12b, and WASP-19b at various phases were reproduced with very good accuracy. It was found that HD189733b has a low Bond albedo and intense heat redistribution, while WASP-19b has a low Bond albedo and low heat redistribution. The exact Roche geometries and temperature distributions over the surface of all 78 transiting extrasolar planets have been determined. Departures from the spherical shape may vary considerably but departures of about 1% in the radius are common within the sample. In some cases, these departures can reach 8%, 12%, or 14%, for WASP-33b, WASP-19b, and WASP-12b, respectively. The mean temperatures of these planets also vary considerably from 300 K to 2600 K. The extreme cases are WASP-18b, WASP-12b, and WASP-33b, with mean temperatures of 2330 K, 2430 K, and 2600 K, respectively.

Key words: binaries: close – binaries: eclipsing – brown dwarfs – planetary systems – stars: low-mass

Online-only material: color figures

1. INTRODUCTION

An interacting binary star is a type of binary star whose components are very close to each other. Strong mutual irradiation, tidal or magnetic interaction between the components take place and these are often accompanied by mass transfer and accretion phenomena. Since the components are very close there is an enhanced probability of eclipses. Such eclipsing binaries provide a unique opportunity to measure the masses and radii of objects with high precision. Transiting extrasolar planets are very similar to these objects and the main difference is only in the very low mass of one of the components.

There are sophisticated computer codes for calculating and inverting light curves or spectra of eclipsing binary stars with various shapes or geometry including the Roche model (Lucy 1968; Wilson & Devinney 1971; Wood 1971; Mochnacki & Doughty 1972; Rucinski 1973; Hill 1979; Popper & Etzel 1981; Zhang et al. 1986; Djurasevic 1992; Drechsel et al. 1994; Linnell & Hubeny 1996; Hadrava 1997; Orosz & Hauschildt 2000; Bradstreet & Steelman 2002; Pribulla 2004; Pavlovski et al. 2006; Tamuz et al. 2006). The Wilson & Devinney (WD) code is most often used and is continuously being improved or modified (Kallrath et al. 1998; Prša & Zwitter 2005). The reflection effect, or the mutual irradiation of two close objects, is taken into account in most of these codes.

The standard model of this effect is described in Wilson (1990) and is understood in the following way: a surface element of object A is irradiated by many surface elements of object B. A fraction of impinging energy called the bolometric albedo (Rucinski 1969) is converted into heat which raises the local temperature and re-radiates the energy on the day side of the object. The rest of the impinging energy is penetrated into the object. Typically, the bolometric albedo is set to 1 for objects with radiative envelopes and 0.5 for objects with convective envelopes (Rucinski 1969). An increase in temperature on the day side of one object triggers a secondary reflection effect on the second object. One, two, or several iterations ("reflections") may be necessary to converge to a final state. The Roche model, limb darkening, and gravity darkening are taken into account. This model does a good job for many interacting binaries and can fit photometric and radial velocity observations of many eclipsing binaries (Wilson 1990, 1994).

However, I argue that the above model of the reflection effect should be revisited. There has been much progress in the field since this standard model of the reflection effect was developed. New types of very cool objects such as brown dwarfs and extrasolar planets have been discovered. These new areas evolve rapidly and produce interesting results. In many respects, a star with a giant close-in planet can be viewed as an "interacting binary." It is thus an attractive idea to apply these new results from the extrasolar planets to interacting binaries and vice versa. For example, models of extrasolar planets take into account day–night heat redistribution and reflected light while models of interacting binaries consider Roche geometry.

The standard model of the reflection effect faces several problems which prevent its application to cool objects irradiated by hot objects and to extrasolar planets. A considerable amount of energy might be reflected off the surface of a very cold

strongly irradiated object. The standard model of the reflection effect in the interacting binaries neglects this reflected light which can be substantial, especially at shorter wavelengths. This reflected light bears the spectroscopic signatures of the hot irradiating star and it is not converted into heat and re-radiated. It is taken into account in models of hot Jupiters or exoplanets (Seager et al. 2000; Sudarsky et al. 2005). The definition of albedo in the planetary sciences is almost the opposite of its meaning for interacting binaries. In planetary studies, the albedo represents a fraction of the impinging energy which is reflected off the object and is not absorbed or converted into heat. Reflected and re-radiated thermal photons may also have completely different Doppler shifts depending on the mutual velocities of the two objects and the observer.

Moreover, some portion of the energy absorbed on the day side can be transferred to and irradiated from the night side. Different parameterizations of this effect in connection with extrasolar planets have been studied by Guillot et al. (1996), Burrows et al. (2006), and Cowan & Agol (2010). Calculations of atmosphere models of extrasolar planets (Hubeny et al. 2003; Barman et al. 2005; Burrows et al. 2008; Fortney et al. 2008) demonstrate that there is a deep temperature plateau which turns off convection in the atmospheres. Convection and vertical energy transport operate only at very deep layers. Observations of hot Jupiters indicate that only a very small fraction of the impinging radiation (10^{-4}) could have penetrated into the object (Burrows et al. 2007). Hydrodynamical simulations and circulation models of the atmospheres of extrasolar planets with various approximations (Dobbs-Dixon & Lin 2008; Showman et al. 2009; Menou & Rauscher 2009) indicate that there are very strong horizontal currents and jets which can effectively redistribute and circulate the energy between the day and night side of the planet, especially along lines of constant latitude. How much energy gets redistributed to the night side depends mainly on the complex structure and dynamics of the surface layers.

On the other hand, most of the transiting exoplanets or giant close-in exoplanets are so close to their host stars that they experience strong tidal effects and their orbit is circular (see references given in Table 1, or Schneider 1995). Rotation of these objects is expected to be synchronous since current theories of tidal circularization and synchronization (Zahn 1977; Tassoul & Tassoul 1992) predict synchronization times much shorter than times needed for circularization of the orbit. Consequently, the shapes of these planets may depart from a sphere or a rotational ellipsoid and may be best described by the Roche model. The above effects and findings must be taken into account in the new or revisited model of the reflection effect, especially when modeling very cold components of interacting binaries or close-in giant extrasolar planets.

The main purpose of this paper is to combine and apply the knowledge from interacting binaries and extrasolar planets and to develop a new model of the reflection effect that can be used to model the cold components of interacting binaries or close-in giant extrasolar planets. The model includes reflected (scattered) light, heating (absorption of the light), heat redistribution over the surface, and Roche geometry. The model was incorporated into the SHELLSPEC code developed by Budaj & Richards (2004) and Budaj et al. (2005). This program was originally designed to calculate light curves, spectra, and images of interacting binaries immersed in a moving circumstellar environment which is optically thin. The code is freely available at http://www.ta3.sk/~budaj/shellspec.html and can be used to study various effects observed or expected in interacting binaries or extrasolar planets. A Fortran90 version of the code which also solves the inverse problem was created by Tkachenko et al. (2010).

2. ROCHE MODEL

In the SHELLSPEC code the Roche model serves as a boundary condition for the radiative transfer in circumstellar matter. Both objects, star and companion, may have shapes according to the Roche model for detached or contact systems. Descriptions of the Roche model can be found in Kopal (1959), Plavec & Kratochvil (1964), and many other papers and books. Let us assume a Cartesian coordinate system (x, y, z) centered on one of the stars (labeled as 1) such that the companion (labeled as 2) is at (1,0,0) and revolves around the z-axis in the direction of the positive y-axis. Let the mass ratio, q, always be m_2/m_1 or "companion/star" and $q < 1$ will indicate the companion is lighter while $q > 1$ means the central star is lighter. Then, the normalized Roche potential, C, is expressed as

$$C(x,y,z) = \frac{2}{(1+q)r_1} + \frac{2q}{(1+q)r_2} + \left(x - \frac{q}{1+q}\right)^2 + y^2, \tag{1}$$

where

$$r_1 = \sqrt{x^2+y^2+z^2}$$
$$r_2 = \sqrt{(x-1)^2+y^2+z^2}. \tag{2}$$

The Roche surface of a detached component is defined as an equipotential surface $C_s = C(x_s, y_s, z_s)$ passing through the sub-stellar point (x_s, y_s, z_s) (point on the surface of the object in between the objects, $0 < x_s < 1$, $y_s = z_s = 0$) which is localized by the "fill-in" parameter $f_i \leqslant 1$. We define this by

$$f_i = x_s/L_{1x}, \quad f_i = (1-x_s)/(1-L_{1x}) \tag{3}$$

for the primary and the secondary, respectively.[1] L_{1x} is the x-coordinate of the L1 point L1$(L_{1x}, 0, 0)$. The above formulation assumes a circular orbit, synchronous rotation, and that the rotation and orbital axes of the detached component are aligned. An illustration of this geometry is depicted in Figure 1.

Derivatives of the Roche potential are

$$C_x = \frac{\partial C}{\partial x}, \quad C_y = \frac{\partial C}{\partial y}, \quad C_z = \frac{\partial C}{\partial z}. \tag{4}$$

Gravity darkening of the non-spherical objects is taken into account by varying the surface temperature according to the von Zeipel law:

$$T/T_p = (g/g_p)^\beta, \tag{5}$$

where g is the normalized surface gravity and β is the gravity darkening coefficient/exponent. This exponent has typical values of 0.08 and 0.25 for convective and radiative envelopes, respectively (von Zeipel 1924; Lucy 1967; Claret 1998). T_p, g_p are the temperature and gravity at the rotation pole, respectively. The normalized gravity vector is $\mathbf{g} = (C_x, C_y, C_z)$ and

$$g = \sqrt{C_x^2 + C_y^2 + C_z^2}. \tag{6}$$

[1] Other definitions of the "filling parameter" in terms of the Roche potential are frequently used.

Table 1
Shapes of the Transiting Exoplanets

Name	a	q	$R_{\rm sub}$	$R_{\rm back}$	$R_{\rm pole}$	$R_{\rm side}$	$R_{\rm eff}$	rr	f_i	$T_{\rm mean}$	Reference
GJ 1214b	0.01400	9186	0.24342	0.24340	0.24088	0.24150	0.24192	1.01053	0.253	551	Charbonneau et al. (2009)
WASP-19b	0.01640	865	1.43896	1.42960	1.28052	1.31000	1.33680	1.12373	0.590	1914	Hebb et al. (2010)
CoRoT-7b	0.01720	64503	0.15108	0.15107	0.14965	0.15000	0.15024	1.00952	0.244	1760	L'eger et al. (2009)
WASP-18b	0.02047	128	1.16966	1.16949	1.16349	1.16500	1.16601	1.00531	0.208	2329	Southworth et al. (2009a)
OGLE-TR-56b	0.02250	949	1.34392	1.34211	1.28736	1.30000	1.30950	1.04393	0.414	1967	Pont et al. (2007)
TrES-3	0.02260	504	1.31652	1.31569	1.28839	1.29500	1.29967	1.02183	0.329	1606	O'Donovan et al. (2007)
WASP-12b	0.02290	1002	1.98765	1.97291	1.74650	1.79000	1.83079	1.13808	0.613	2407	Hebb et al. (2009)
OGLE-TR-113b	0.02290	618	1.10252	1.10213	1.08607	1.09000	1.09273	1.01515	0.290	1114	Gillon et al. (2006)
WASP-4b	0.02300	840	1.46767	1.46538	1.40130	1.41600	1.42715	1.04736	0.425	1815	Southworth et al. (2009b)
CoRoT-1b	0.02540	966	1.54395	1.54167	1.47462	1.49000	1.50166	1.04702	0.424	1835	Barge et al. (2008)
WASP-33b	0.02560	1410	1.66033	1.65542	1.53414	1.56000	1.58143	1.08225	0.512	2582	Collier Cameron et al. (2010)
WASP-5b	0.02729	653	1.18130	1.18101	1.16773	1.17100	1.17325	1.01162	0.266	1737	Southworth et al. (2009c)
CoRoT-2b	0.02810	306	1.47584	1.47548	1.46154	1.46500	1.46736	1.00979	0.253	1495	Alonso et al. (2008)
GJ 436b	0.02872	6574	0.43970	0.43968	0.43744	0.43800	0.43838	1.00516	0.200	695	Bean et al. (2008)
SWEEPS-11	0.03000	118	1.13119	1.13116	1.12961	1.13000	1.13026	1.00140	0.134	1959	Sahu et al. (2006)
OGLE-TR-132b	0.03060	1157	1.19343	1.19309	1.17577	1.18000	1.18294	1.01503	0.288	1925	Gillon et al. (2007)
HD 189733b	0.03099	741	1.14505	1.14488	1.13573	1.13800	1.13955	1.00821	0.236	1178	Bouchy et al. (2005)
WASP-2b	0.03138	962	1.02260	1.02249	1.01519	1.01700	1.01823	1.00730	0.227	1258	Daemgen et al. (2009)
WASP-3b	0.03170	737	1.32162	1.32131	1.30630	1.31000	1.31254	1.01172	0.266	1930	Gibson et al. (2008)
TrES-2	0.03556	856	1.28042	1.28022	1.26929	1.27200	1.27385	1.00876	0.241	1455	Daemgen et al. (2009)
WASP-24b	0.03590	1145	1.11018	1.11006	1.10200	1.10400	1.10536	1.00742	0.228	1611	Street et al. (2010)
XO-2b	0.03690	1800	0.97839	0.97830	0.97126	0.97300	0.97419	1.00735	0.226	1281	Burke et al. (2007)
WASP-14b	0.03700	178	1.26047	1.26044	1.25851	1.25900	1.25932	1.00156	0.138	1802	Joshi et al. (2008)
WASP-10b	0.03710	243	1.08107	1.08105	1.07965	1.08000	1.08024	1.00132	0.130	1008	Johnson et al. (2009)
HAT-P-7b	0.03790	855	1.43186	1.43160	1.41753	1.42100	1.42338	1.01011	0.253	2075	Welsh et al. (2010)
WASP-1b	0.03820	1459	1.37324	1.37289	1.35319	1.35800	1.36134	1.01482	0.287	1749	Collier Cameron et al. (2007)
HAT-P-12b	0.03840	3623	0.96819	0.96804	0.95607	0.95900	0.96102	1.01267	0.271	930	Hartman et al. (2009)
HAT-P-3b	0.03894	1636	0.89290	0.89285	0.88905	0.89000	0.89064	1.00432	0.190	1119	Torres et al. (2007)
TrES-1	0.03930	1493	1.08664	1.08654	1.07917	1.08100	1.08224	1.00692	0.222	1050	Alonso et al. (2004)
WASP-26b	0.04000	1150	1.32922	1.32902	1.31704	1.32000	1.32202	1.00924	0.245	1615	Smalley et al. (2010)
HAT-P-5b	0.04075	1146	1.26718	1.26704	1.25768	1.26000	1.26158	1.00755	0.229	1496	Bakos et al. (2007a)
OGLE-TR-10b	0.04162	1961	1.27165	1.27142	1.25629	1.26000	1.26256	1.01223	0.268	1238	Pont et al. (2007)
WASP-6b	0.04210	2456	1.23659	1.23635	1.22000	1.22400	1.22677	1.01360	0.278	1353	Gillon et al. (2009)
WASP-16b	0.04210	1251	1.01088	1.01084	1.00706	1.00800	1.00864	1.00380	0.182	1235	Lister et al. (2009)
HAT-P-13b	0.04260	1503	1.28881	1.28863	1.27717	1.28000	1.28194	1.00911	0.243	1600	Bakos et al. (2009a)
HD 149026b	0.04313	3792	0.65543	0.65542	0.65353	0.65400	0.65432	1.00291	0.165	1700	Sato et al. (2005)
HAT-P-10b	0.04390	1867	1.04940	1.04933	1.04357	1.04500	1.04597	1.00558	0.206	1004	Bakos et al. (2009b)
HAT-P-4b	0.04460	1940	1.27961	1.27944	1.26692	1.27000	1.27211	1.01002	0.251	1641	Kovacs et al. (2007)
XO-3b	0.04540	107	1.21742	1.21741	1.21686	1.21700	1.21709	1.00046	0.092	1662	Johns-Krull et al. (2008)
WASP-28b	0.04550	1243	1.12346	1.12340	1.11887	1.12000	1.12076	1.00410	0.187	1375	West et al. (2010)
Kepler-4b	0.04560	16634	0.35747	0.35747	0.35684	0.35700	0.35710	1.00175	0.139	1570	Borucki et al. (2010a)
WASP-29b	0.04560	3479	0.74182	0.74181	0.73940	0.74000	0.74040	1.00328	0.172	970	Hellier et al. (2010)
Kepler-6b	0.04567	1892	1.33329	1.33310	1.31970	1.32300	1.32526	1.01030	0.253	1461	Dunham et al. (2010)
Lupus-TR-3b	0.04640	1124	0.89117	0.89115	0.88961	0.89000	0.89026	1.00175	0.140	987	Weldrake et al. (2008)
WASP-22b	0.04680	2057	1.12528	1.12520	1.11828	1.12000	1.12116	1.00626	0.214	1384	Maxted et al. (2010)
OGLE-TR-111b	0.04700	1620	1.07037	1.07032	1.06590	1.06700	1.06774	1.00419	0.188	987	Pont et al. (2004)
HD 209458b	0.04707	1544	1.32755	1.32742	1.31756	1.32000	1.32166	1.00759	0.229	1375	Henry et al. (2000)
WASP-25b	0.04740	1805	1.26718	1.26705	1.25768	1.26000	1.26158	1.00755	0.228	1207	Enoch et al. (2010)
Kepler-8b	0.04830	2106	1.43187	1.43162	1.41490	1.41900	1.42183	1.01200	0.266	1616	Jenkins et al. (2010)
XO-5b	0.04870	855	1.09073	1.09070	1.08843	1.08900	1.08938	1.00211	0.150	1207	Burke et al. (2008)
HAT-P-8b	0.04870	882	1.50647	1.50635	1.49790	1.50000	1.50142	1.00573	0.209	1658	Latham et al. (2009)
XO-1b	0.04880	1163	1.18727	1.18722	1.18293	1.18400	1.18472	1.00367	0.180	1208	McCullough et al. (2006)
CoRoT-5b	0.04947	2242	1.39965	1.39943	1.38428	1.38800	1.39056	1.01110	0.259	1400	Rauer et al. (2009)
WASP-15b	0.04990	2280	1.44095	1.44071	1.42387	1.42800	1.43085	1.01200	0.266	1607	West et al. (2009)
Kepler-5b	0.05064	680	1.43466	1.43459	1.42980	1.43100	1.43180	1.00340	0.176	1758	Borucki et al. (2010b)
TrES-4	0.05091	1577	1.82048	1.81998	1.79224	1.79900	1.80371	1.01576	0.292	1705	Daemgen et al. (2009)
OGLE-TR-211b	0.05100	1352	1.36583	1.36573	1.35810	1.36000	1.36128	1.00569	0.208	1683	Udalski et al. (2008)
OGLE-TR-182b	0.05100	1182	1.13241	1.13238	1.12921	1.13000	1.13053	1.00284	0.165	1315	Pont et al. (2008)
WASP-17b	0.05100	2564	1.77093	1.77022	1.73048	1.74000	1.74678	1.02337	0.333	1594	Anderson et al. (2010a)
WASP-21b	0.05200	3526	1.07550	1.07543	1.06821	1.07000	1.07121	1.00682	0.220	1229	Bouchy et al. (2010)
HAT-P-6b	0.05235	1278	1.33465	1.33457	1.32848	1.33000	1.33102	1.00464	0.194	1628	Noyes et al. (2008)
WASP-13b	0.05270	2937	1.21722	1.21711	1.20767	1.21000	1.21159	1.00791	0.231	1439	Skillen et al. (2009)
HAT-P-9b	0.05300	1718	1.40744	1.40731	1.39759	1.40000	1.40164	1.00705	0.223	1487	Shporer et al. (2009)
HAT-P-11b	0.05300	10473	0.45248	0.45248	0.45184	0.45200	0.45211	1.00142	0.130	844	Bakos et al. (2010)
SWEEPS-04	0.05500	341	0.81015	0.81014	0.80995	0.81000	0.81003	1.00024	0.073	1348	Sahu et al. (2006)
HAT-P-1b	0.05530	2264	1.23003	1.22996	1.22336	1.22500	1.22611	1.00545	0.205	1259	Bakos et al. (2007b)

Table 1
(Continued)

Name	a	q	$R_{\rm sub}$	$R_{\rm back}$	$R_{\rm pole}$	$R_{\rm side}$	$R_{\rm eff}$	rr	f_i	$T_{\rm mean}$	Reference
XO-4b	0.05550	803	1.34252	1.34248	1.33917	1.34000	1.34055	1.00250	0.159	1414	McCullough et al. (2008)
CoRoT-3b	0.05700	66	1.01006	1.01006	1.00998	1.01000	1.01001	1.00008	0.052	1656	Deleuil et al. (2008)
HAT-P-14b	0.06060	650	1.15084	1.15083	1.14972	1.15000	1.15019	1.00098	0.116	1525	Torres et al. (2010)
WASP-7b	0.06180	1396	0.91568	0.91568	0.91477	0.91500	0.91515	1.00099	0.116	1344	Hellier et al. (2009)
Kepler-7b	0.06224	3258	1.48887	1.48871	1.47451	1.47800	1.48040	1.00974	0.248	1514	Latham et al. (2010)
HAT-P-2b	0.06878	156	1.15714	1.15714	1.15695	1.15700	1.15703	1.00016	0.065	1442	Pál et al. (2010)
WASP-8b	0.07930	485	1.17030	1.17030	1.16990	1.17000	1.17007	1.00034	0.082	912	Smith et al. (2009)
CoRoT-6b	0.08550	373	1.16618	1.16618	1.16594	1.16600	1.16604	1.00021	0.070	990	Fridlund et al. (2010)
CoRoT-4b	0.09000	1600	1.19072	1.19072	1.18976	1.19000	1.19016	1.00081	0.108	1039	Moutou et al. (2008)
HD 17156b	0.16230	404	1.02302	1.02302	1.02299	1.02300	1.02300	1.00002	0.033	852	Winn et al. (2009)
CoRoT-9b	0.40700	1234	1.05000	1.05000	1.05000	1.05000	1.05000	1.00000	0.019	401	Deeg et al. (2010)
HD 80606b	0.44900	239	0.92100	0.92100	0.92100	0.92100	0.92100	1.00000	0.009	365	Fossey et al. (2009)

Notes. Columns are: a -semi-major axis in [AU], q -star/planet mass ratio, $R_{\rm sub}$ -planet radius at the sub-stellar point ($R_{\rm sub}$,0,0), $R_{\rm back}$ -planet radius at the anti-stellar point, $R_{\rm pole}$ -planet radius at the rotation pole (0,0,$R_{\rm pole}$), $R_{\rm side}$ -planet radius at the side point (0,$R_{\rm side}$,0), (assumed equal to the planet radius determined from the transit), $R_{\rm eff}$ -effective radius of the planet, $rr = R_{\rm sub}/R_{\rm pole}$ -departure from the sphere, $f_i = R_{\rm sub}/L_{1x}$ -fill-in parameter of the Roche lobe, $T_{\rm mean}$ -mean temperature of the planet in K. Radii are in units of Jupiter radius. Coordinates of the center of mass of the planet are (0,0,0). See the text for a more detailed information.

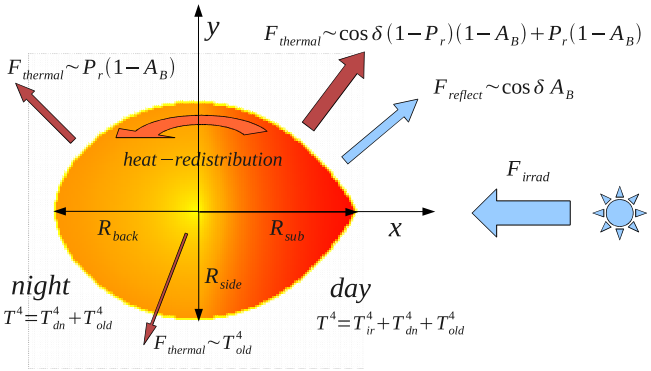

Figure 1. Schematic illustration of the reflection effect which consists of reflection, heating, and heat redistribution. This is a pole-on view of the planet irradiated by the star. Red regions on the day side are hot while yellow regions on the night side and around poles are cool due to the irradiation and zonal heat transfer. δ is irradiating angle, A_B is Bond albedo, P_r is heat redistribution parameter, $T_{\rm ir}$ is temperature associated with local heating, $T_{\rm dn}$ is associated with heat redistribution and is a function of latitude, and $T_{\rm old}$ is associated with surface temperatures in the absence of the irradiation. The Roche shape of the planet corresponds to the filling factor equal to 1. The position and size of the star are not to scale.

(A color version of this figure is available in the online journal.)

Limb darkening is taken into account using the quadratic limb-darkening law,

$$I(\theta) = I(0) f_{\rm LD} \tag{7}$$

$$f_{\rm LD} = 1 - u_1(1-\cos\theta) - u_2(1-\cos\theta)^2, \tag{8}$$

and by calculating the cosine of the angle θ between the line-of-sight unit vector $\mathbf{n} = (n_x, n_y, n_z)$ and a normal to the surface:

$$\cos\theta = -\mathbf{n}.\mathbf{g}/g = -\frac{n_x C_x + n_y C_y + n_z C_z}{\sqrt{C_x^2 + C_y^2 + C_z^2}}. \tag{9}$$

$I(0)$ is intensity perpendicular to the surface.

3. IRRADIATION AND HEAT REDISTRIBUTION

In this section, we will describe our treatment of the mutual irradiation of the objects. It can be applied to both objects, but we will neglect multiple reflections between the two objects since this is not essential if one of them is much less luminous. We will distinguish between three separate processes: **reflection** of the light off the object (or scattering which does not produce any **heating** of the irradiated surface), heating of the irradiated surface (day side) by the absorbed light, and subsequent **heat redistribution** over the entire surface of the object. Let us assume that the day side of a planet is irradiated by the star; then the impinging flux at a location $\mathbf{r}$ from star at $\mathbf{r}_*$ is

$$F_{\rm ir} = \cos\delta \frac{R_\star^2}{(\mathbf{r}-\mathbf{r}_*)^2} \sigma T_\star^4, \tag{10}$$

where $R_\star$, $T_\star$ are radius and effective temperature of the star, respectively, and δ is an irradiating angle which is the zenith distance of the center of the star as seen from the surface of the planet:

$$\cos\delta = \frac{(\mathbf{r}-\mathbf{r}_*).\mathbf{g}}{|\mathbf{r}-\mathbf{r}_*|g} = \frac{(r_x - r_{x*})C_x + (r_y - r_{y*})C_y + (r_z - r_{z*})C_z}{|\mathbf{r}-\mathbf{r}_*|\sqrt{C_x^2 + C_y^2 + C_z^2}}. \tag{11}$$

Now let us define two local parameters $A_B(\alpha, \beta)$, $P_r(\alpha, \beta)$ on the day side of the planet (irradiated side of an object) where α, β are the longitude and the latitude, respectively, measured from the sub-stellar point. P_r will be the local heat redistribution parameter and A_B will be the local Bond albedo of the surface. Consequently, $A_B F_{\rm ir}$ is the flux immediately reflected off the surface, $(1-A_B)F_{\rm ir}$ will be the fraction of the irradiating energy which is absorbed and converted into heat, $P_r(1-A_B)F_{\rm ir}$ will be the part of the latter which is redistributed over the day and night side of the object, while the remaining part, $(1-P_r)(1-A_B)F_{\rm ir}$, will heat the local area.[2] Then the energy conservation for the day–night heat transport can be written as

$$\iint P_r(1-A_B)F_{\rm ir} dS_{\rm day} = \iint \sigma T_{\rm dn}^4 dS_{\rm day+night}. \tag{12}$$

[2] Note that our local P_r parameter should not be confused with the global P_n parameter of Burrows et al. (2006). P_n is a fraction of the impinging stellar radiation which is transferred to and re-radiated from the night side, $P_n \approx P_r(1-A_B)/2$. P_n is from the interval 0–0.5 while P_r runs from 0 to 1. P_r is a direct indicator of the heat redistribution while the P_n parameter only reflects a combination of the heat redistribution and Bond albedo.

Let us assume, for simplicity (or in the absence of a better approximation), that $A_B(\alpha,\beta)$, $P_r(\alpha,\beta)$ are constant and the heat is homogeneously redistributed over the day and night sides so that the surface has a constant temperature T_0. Then,

$$P_r(1-A_B)\iint F_{\rm ir} dS_{\rm day} \Big/ \iint dS_{\rm day+night} = \sigma T_0^4. \quad (13)$$

In the case that the planet has a spherical shape and is far from the star, this reduces to

$$T_0^4 = \frac{1}{4} P_r (1-A_B)\frac{R_\star^2}{d^2} T_\star^4. \quad (14)$$

Let us explore another case, namely, that the horizontal circulation on the planet along the lines of constant latitude is so strong that it dominates the day–night heat transport and the equilibrium surface temperature, T_1, will be a function of latitude. In this case and with the assumptions above (spherical planet far from the star), one can consider an energy conservation for a fixed latitude:

$$P_r(1-A_B)\int F_{\rm ir}\cos(\beta) d\alpha = \sigma T_1^4(\beta)\int \cos(\beta) d\alpha, \quad (15)$$

where

$$\cos(\delta) = \cos(\alpha)\cos(\beta). \quad (16)$$

The solution is that the temperature depends on the fourth root of $\cos(\beta)$:

$$T_1^4(\beta) = \frac{1}{\pi} P_r (1-A_B)\frac{R_\star^2}{d^2} T_\star^4 \cos(\beta) = \frac{4}{\pi} T_0^4 \cos(\beta). \quad (17)$$

The study of these two extreme cases leads us to suggest a heat redistribution model in which the day–night heat transport is a combination of the two cases mentioned above. Namely, we will express the surface temperature in the following way:

$$T_{\rm dn}^4(\beta) = T_0^4[P_a + P_b\cos(\beta)], \quad (18)$$

where P_a, P_b are the "zonal temperature redistribution parameters." $P_a = \langle 0,1\rangle$ and P_b is to be determined from Equation (12) so that the total energy budget is conserved. From Equations (12), (13), and (18) we obtain

$$P_b = (1-P_a)\frac{\iint dS_{\rm day+night}}{\iint \cos\beta dS_{\rm day+night}}. \quad (19)$$

It can be shown that in the case of a spherical planet far from its star

$$P_b = \frac{4}{\pi}(1-P_a) \quad (20)$$

and $P_b = \langle 0, 4/\pi\rangle$. Note that P_a is a measure of the effectiveness of the homogeneous temperature distribution over the surface versus the zonal distribution. It is intimately linked with the effectiveness of the heat flows along the meridians versus parallels.[3]

Finally, the temperature distribution on the surface of the irradiated planet will be

$$T^4 = T_{\rm ir}^4 + T_{\rm dn}^4 + T_{\rm old}^4, \quad (21)$$

where

$$T_{\rm ir}^4 = (1-P_r)(1-A_B)F_{\rm ir}/\sigma, \quad T_{\rm ir}^4 = 0 \quad (22)$$

on the day and night side, respectively. $T_{\rm old}$ is the prior temperature distribution over the surface in the absence of the irradiation (including gravity darkening, etc.) given by Equation (5). In the absence of gravity darkening, $T_{\rm old}$ represents the intrinsic cooling of the object measured at its surface. It should be noted that imposing the external irradiation on one side of the object can alter the original temperature distribution (cooling). Budaj et al. (2010) argue that the core cooling rates ($T_{\rm old}$) from the day and night side of a strongly irradiated planet may not be the same and that the difference depends on several important parameters, such as the effectiveness and the depth where the day–night heat transport occurs, the stellar irradiation flux, and vertical redistribution of the opacities, atmospheric abundances, and/or presence of the stratospheres.

Once we know the temperature distribution over the surface, we can approximate the monochromatic flux from the surface as being composed of two parts:

$$F_\nu = F_\nu^{\rm reflect} + F_\nu^{\rm thermal}. \quad (23)$$

Reflection depends on the surface albedo A_ν and has to take into account the mutual velocities of the star, planet, and the observer:

$$F_\nu^{\rm reflect} = A_{\nu_2} F_{\nu_1 {\rm ir}} \quad (24)$$

$$F_{\nu_1 {\rm ir}} = \cos\delta \frac{R_\star^2}{(\mathbf{r}-\mathbf{r}_*)^2} F_{\nu_1}^\star, \quad (25)$$

where $F_{\nu_1}^\star$ is flux emerging from the surface of the irradiating star. The Doppler shifts corresponding to the mutual velocities of the objects and observer are the following:

$$\nu_2 = \nu\left(1 - \frac{v_z}{c}\right) \quad (26)$$

$$\nu_1 = \nu\left(1 - \frac{v_z + v_2}{c}\right) \quad (27)$$

$$v_2 = -\frac{(\mathbf{r}-\mathbf{r}_\star).(\mathbf{v}-\mathbf{v}_\star)}{|\mathbf{r}-\mathbf{r}_\star|}, \quad (28)$$

where $\mathbf{v}$ is the velocity field vector at the given point on the irradiated surface specified by the vector $\mathbf{r}$, $\mathbf{v}_\star$ is the velocity of the center of mass of the irradiating star, and the z-coordinate points to the observer. In this way, we fully take into account the mutual velocities of the objects and observer as well as rotation of the reflecting object.[4] To calculate the reflected intensity we assume that the reflection is isotropic, in which case

$$I_\nu^{\rm reflect} = F_\nu^{\rm reflect}/\pi. \quad (29)$$

Finally, we assume that $F_\nu^{\rm thermal}$ can be approximated by the flux emerging from the non-irradiated model atmosphere[5] with

[3] Note that a temperature distribution with hotter poles might be modeled using $P_a > 1$ and $P_b < 0$.

[4] Note that Doppler shifts in the scattered and thermal radiation may not be the same and may not be trivial. A more detailed treatment would require high-resolution radiative transfer in the irradiated atmospheres for a set of radial planet–star velocities.

[5] This approximation is also used in the standard model of the reflection effect and many other codes for eclipsing binaries. It works well for many interacting binaries (Wilson 1990). The reason for such an approximation is that calculations of irradiated models and emerging intensities are not simple (see irradiated models of interacting binaries by Rucinski 1970, 1973b and Vaz & Norlund 1985), and are beyond the scope of this paper. There are cases when this approximation may not work very well, for example, for hot Jupiters with pronounced stratospheres.

an effective temperature equal to the surface temperature of the irradiated object given by Equation (21):

$$F_{\nu}^{\rm thermal} = F_{\nu_2}(T_{\rm eff} = T) \tag{30}$$

and the associated intensity is given by

$$I_{\nu}^{\rm thermal} = I_{\nu}(0)^{\rm thermal} f_{\rm LD} \tag{31}$$

$$I_{\nu}(0)^{\rm thermal} = \frac{F_{\nu}^{\rm thermal}}{\pi(1 - u_1/3 - u_2/6)}. \tag{32}$$

In this way, we also take into account the limb darkening of the reflecting object.

Local Bond albedo used here is a weighted monochromatic albedo A_ν:

$$A_B = \frac{\int A_\nu F_\nu^\star d\nu}{\int F_\nu^\star d\nu}. \tag{33}$$

One has to keep in mind that our albedo refers to the reflected light only (not to the absorbed and re-radiated light). If the irradiated object is very cold compared to the irradiating object there is a clear distinction between its thermal radiation and reflected radiation. However, if the two objects have comparable temperatures it is almost impossible to distinguish whether a particular photon was scattered or absorbed and re-radiated. In this case, it is still possible to use our formalism and, e.g., approximate the albedo by using a single scattering albedo to cope with the problem.

It might be convenient to define the mean temperature of the whole distorted object:

$$T_{\rm mean}^4 \equiv \frac{\int T^4 dS}{\int dS}, \tag{34}$$

where dS is the surface element of the irradiated object. Note that reflected light does not contribute to the mean temperature. It should not be confused with the effective temperature or brightness temperature.

4. APPLICATION TO EXTRASOLAR PLANETS

Close-in extrasolar planets are an attractive test bed for such models. They are a natural extension of interacting binaries toward cool and small mass companions. Their radiation is governed by the stellar insolation. Atmosphere models of exoplanets which assume/take into account radiative and hydrostatic equilibrium, irradiation, convection, day–night heat redistribution, clouds, and/or nonequilibrium chemistry have been developed (Hauschildt et al. 1999; Seager et al. 2000; Hubeny et al. 2003; Barman et al. 2005; Burrows et al. 2008; Fortney et al. 2008). Models with two-dimensional radiative transfer and dust phase functions were constructed by Sudarsky et al. (2005). At the same time, models with various simplifications are often very useful for studying larger samples of objects and/or many special effects (Hansen 2008; Kipping & Tinetti 2010; Madhusudhan & Seager 2009; Cowan & Agol 2010).

4.1. Shapes of the Transiting Extrasolar Planets

Our knowledge of the size of exoplanets comes mainly from observations of transits. Most exoplanet studies assume that exoplanets have a spherical shape. The precision of photometric measurements is advancing, revealing more and more details. Recently, Kipping & Tinetti (2010) attempted to model the light curve and transit assuming a spherical shape but taking into account the intrinsic night side emission of the planet during the transit. They found that in the infrared region the effect is of the order of 10^{-4}. Seager & Hui (2002), Barnes & Fortney (2003), and Carter & Winn (2010) assumed the shape of a rotational ellipsoid. Welsh et al. (2010) used the Roche potential approximation to describe the shape of the parent star and to explain the ellipsoidal variations of HAT-P-7. Nevertheless, many transiting exoplanets are so close to their host stars that their shape is best described by the Roche model. Very recently, Li et al. (2010) developed a model for the tidally distorted exoplanet WASP-12b which includes mass transfer and circumstellar (planetary) matter.

Our code was applied to transiting extrasolar planets and the exact Roche model shape of all the transiting exoplanets was calculated. A circular orbit with a radius equal to the semi-major axis, and synchronized rotation of the planet, were assumed. This is a very good approximation for transiting exoplanets since the great majority of them indeed have circular orbits (only 10 out of 78 planets studied here have eccentricities larger than 0.1). The results are displayed in Table 1. It lists $R_{\rm sub}$, $R_{\rm back}$, $R_{\rm pole}$, $R_{\rm side}$, and $R_{\rm eff}$ which are the radii at the sub-stellar point, anti-stellar point, rotation pole, on the side, and the effective radius of the planet, i.e., the radius of the sphere with the same volume as the Roche surface, respectively. Departures from the sphere are measured by the value of $R_{\rm sub}/R_{\rm pole}$. It was also assumed that the observed radius of the planet is equal to $R_{\rm side}$ which has almost no effect on the relative proportions (shape) of the planet but may slightly underestimate the departures from the sphere for a few highly distorted planets.

One can see that the departures from the spherical shape vary by several orders of magnitude. Departures of about 1% are common. About 8% of planets (all of them have semi-major axis smaller than 0.03 AU) have departures larger than 3%. These include OGLE-TR-56b, WASP-4b, and CoRoT-1b. The extreme cases are WASP-12b, WASP-19b, and WASP-33b when the departures can exceed 14%, 12%, and 8%, respectively. This is clearly comparable to the precision of the planet radius determination or the transit radius effect. The highest departures seem to be along the line joining the objects (the $R_{\rm sub}/R_{\rm pole}$ parameter) which would mainly affect the overall light curve. During the transit event, it is mainly the $R_{\rm side}/R_{\rm pole}$ parameter which is most relevant and this does not acquire such high values (about 2% in the case of WASP-12b, WASP-19b, and WASP-33b).

The observed radius of the planet should be associated with the cross section of the planet during the transit which is represented by $R_{\rm side}$, $R_{\rm pole}$. On the other hand, the theoretical radius, e.g., from the evolutionary calculations, might be associated more with the effective radius of the planet. One has to keep the findings above in mind when interpreting the planet radius measurements or calculations (Guillot & Showman 2002; Burrows et al. 2007; Fortney et al. 2007; Baraffe et al. 2008; Leconte et al. 2010).

Apart from the shape of these planets, I also calculated a temperature distribution over the surface for all these exoplanets. This is rather cumbersome to tabulate and the result depends heavily on the free parameters of the model which is why I provide the reader with the code which can do that. In Table 1, only the mean temperature of each transiting planet is listed. This was calculated assuming its Roche shape and $A_B = 0.1$, $P_r = 0.5$, $P_a = 0.5$. If not mentioned explicitly

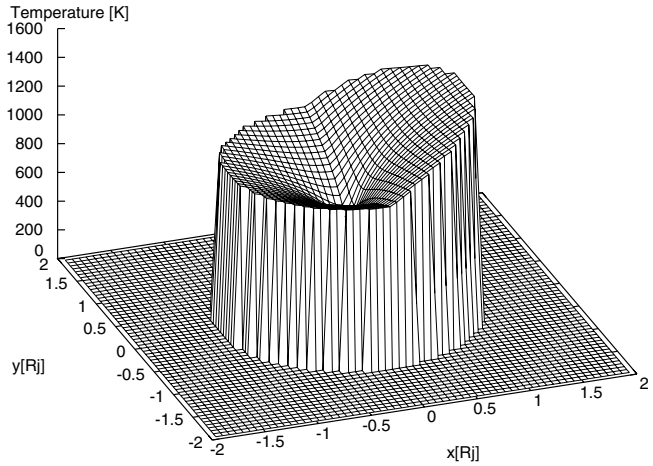

Figure 2. Example of a two-dimensional projection map of the surface temperature of HD189733b calculated for $P_r = 0.6$, $P_a = 0.1$. x-axis points to the star, z-axis to the rotation pole. One can clearly see the hot region on the day side of the planet facing the star. The night side has a non-zero temperature due to the efficient heat redistribution ($P_r = 0.6$). The temperature at the polar region, $(x, y) = (0, 0)$, drops significantly since the heat is redistributed efficiently along parallels but much less effectively along the meridians ($P_a = 0.1$).

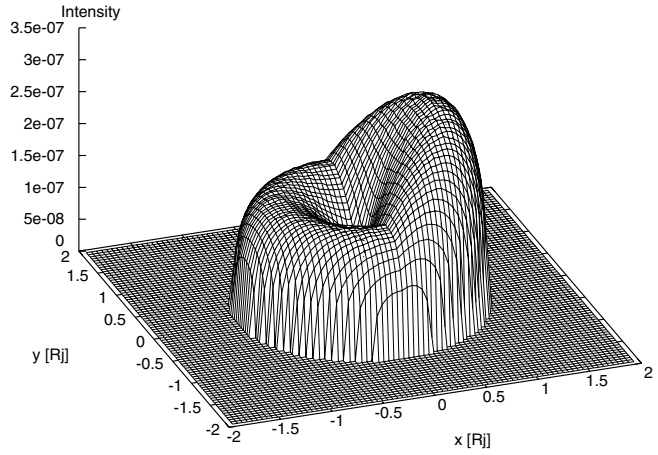

Figure 3. Example of a two-dimensional projection image of HD189733b at 8 μm seen pole-on. The surface intensity is in erg s^{-1} Hz^{-1} cm^{-2} sterad^{-1}. It corresponds to the temperate distribution from Figure 2. The limb darkening ($u_1 = 0.6$, $u_2 = 0.2$) was applied to it. Note that hot regions are now actually dark due to the limb darkening.

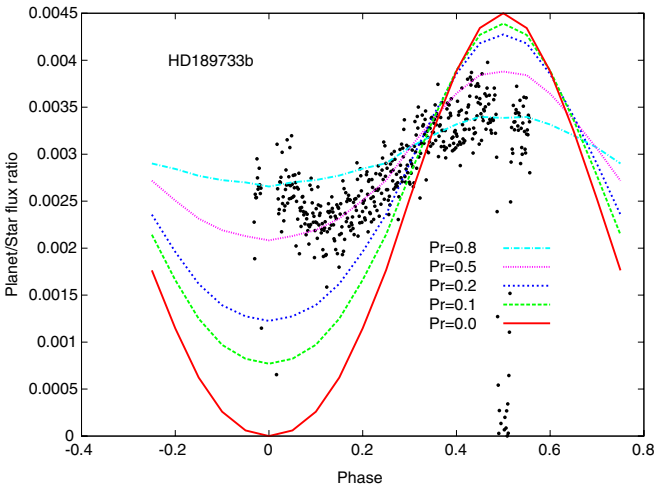

Figure 4. Theoretical light curves of HD189733b compared with the observations of Knutson et al. (2007) at 8 μm (black points). Note the strong dependence on the heat redistribution parameter, P_r, which could reach several orders of magnitude at phase zero. $A_B = 0$, $P_a = 1.0$, and zero limb darkening were assumed.

(A color version of this figure is available in the online journal.)

I also assume $T_{\rm old} = 100$ K.[6] These mean temperatures vary considerably from 300 to 2600 K. The hottest planets are WASP-33b, WASP-12b, and WASP-18b with mean temperatures of about 2600, 2430, and 2330 K, respectively. The separation of these extremely hot planets from the host star is smaller than 0.03 AU and temperatures of planets at a wider separation decrease accordingly.

4.2. Light Curves of the Close-in Extrasolar Planets

In this section, we apply our model to the light curves of transiting extrasolar planets HD189733b and Wasp-12b. We will start with HD189733b. The planet properties were determined by Winn et al. (2007). Knutson et al. (2007) obtained a superb light curve of the planet which covers more than half of its orbit. It was observed at 8 μm in the infrared region.

First, let us introduce the qualitative distribution of the temperature over the surface of HD189733b produced by our model. Figure 2 illustrates the behavior of the temperature for a relatively intense heat redistribution factor $P_r = 0.6$ and quite small zonal temperature redistribution parameter $P_a = 0.1$ (i.e., intense flows along parallels but not very intense heat flows along meridians). One can observe that this model produces hotter regions at the sub-stellar point and near the equator while cooler regions are at the poles. Figure 3 then illustrates the behavior of the intensity. This is what an observer would see looking on the planet pole-on. Limb darkening was applied to the model. One would see the dark polar regions; however, the hot sub-stellar point would not be the brightest since all hotter equatorial regions would be dim due to the limb darkening. The blackbody approximation was used to model the energy distribution.[7]

Now, we can proceed to a comparison between the observations of Knutson et al. (2007) and the models produced by SHELLSPEC shown in Figure 4. The synthetic light curves are very sensitive to the heat redistribution parameter $P_r = \langle 0, 1 \rangle$, especially at phases close to the transit; when the night side of the planet is seen, the flux can change by the orders of magnitude. The best fit is obtained for $P_r = 0.5$–0.8, which means that the surface heat redistribution is crucial and quite effective. This finding is in agreement with the results of Knutson et al. (2007), Burrows et al. (2008), Madhusudhan & Seager (2009), and Cowan & Agol (2010).

Albedo is an important parameter at all wavelengths. The effect of the wavelength-independent Bond albedo is illustrated in Figure 5. Our models indicate that the Bond albedo of this

[6] Most of the transiting exoplanets are hot Jupiters. In the absence of the irradiation, these objects would have an effective temperature similar to that of Jupiter, i.e., of the order of 100 K. This temperature also represents their intrinsic cooling rate.

[7] The main point of this section is to demonstrate and explain the effects of Roche geometry, heat redistribution, albedo, limb darkening/brightening on two-dimensional projection images, and light curves of hot Jupiters. It is desirable to do this in the simplest way to reduce other disturbing features which might mask the effects we are interested in. That is why the blackbody approximation was used if not specified otherwise. Light curves and two-dimensional projected images of hot Jupiters might be difficult to comprehend if they also involved rather complicated interference between the Doppler shifts and high-resolution spectra of the star and planet.

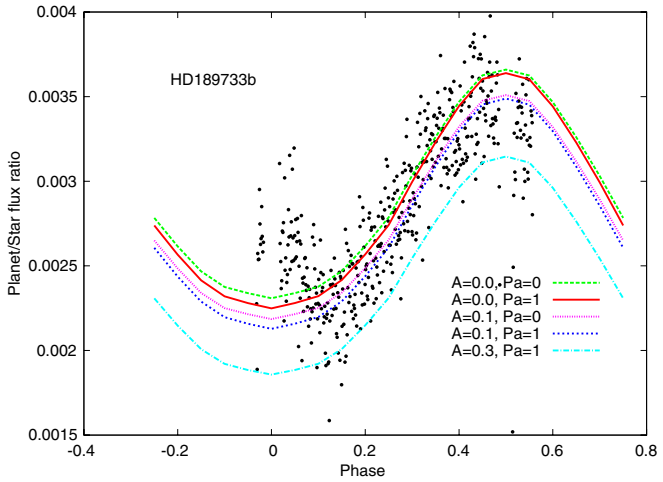

Figure 5. Effect of the Bond albedo and zonal temperature distribution on the light curve of transiting exoplanet HD189733b at 8 μm. A higher Bond albedo reflects more light which is seen mainly at shorter wavelengths. Consequently, less energy is available to be absorbed and redistributed over the surface. Temperatures are lower which means lower fluxes in the IR region. If $P_a = 0$ and the heat flows mainly along the parallels then (compared to the homogeneous flows with $P_a = 1$) one would detect slightly more light at all phases, especially on the night side. Black points are the observations of Knutson et al. (2007). $P_r = 0.6$ and zero limb darkening were assumed.

(A color version of this figure is available in the online journal.)

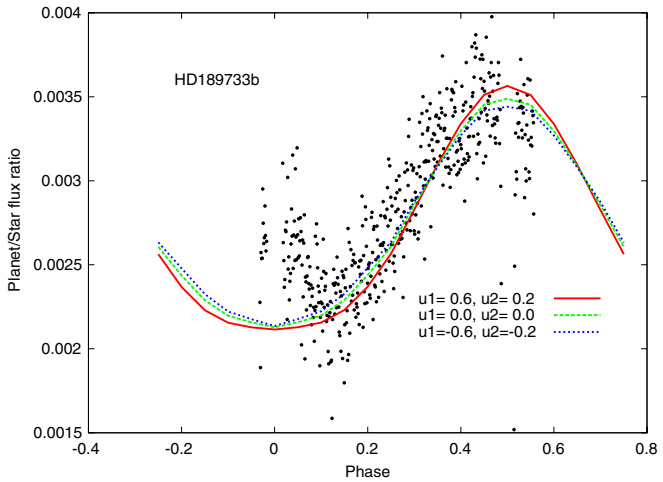

Figure 6. Effect of the limb darkening/brightening on the theoretical light curve of the transiting exoplanet HD189733b at 8 μm. Limb darkening has almost no effect at phase zero but much stronger effect shortly before and after the transit and near the secondary eclipse. This is because when we observe the night side with almost constant temperature distribution the darkening at the limb is compensated by the brightening at the center to conserve the flux. However, during the secondary eclipse the limb darkening suppresses the radiation from the cold regions and amplifies the radiation from the hot regions. The net effect is that planet is brighter at the phase 0.5. The opposite happens shortly before and after the transit. Limb brightening has the opposite behavior. Black points are the observations of Knutson et al. (2007). $A_B = 0.1$, $P_r = 0.6$, $P_a = 1.0$ were assumed.

(A color version of this figure is available in the online journal.)

planet is relatively small at about 0.1 which is in agreement with Cowan & Agol (2010). Higher albedo reflects more light, which could be observed especially at shorter wavelengths. This reflected light might be relatively small in the IR region. However, higher albedo reduces the amount of energy absorbed and redistributed over the surface. Surface temperatures are lower which manifests in lower fluxes at longer wavelengths.

It is interesting to see that these kinds of light curves of transiting exoplanets are not very sensitive to the zonal temperature redistribution parameter $P_a = \langle 0, 1 \rangle$ associated with the effectiveness of the homogeneous heat transfer versus zonal transfer. This is also illustrated in Figure 5. If the heat flows mainly along the equator and not along the meridians ($P_a = 0$) and we view the planet almost edge-on then we observe a slight increase of flux at all phases, especially on the night side (compared to the homogeneous temperature distribution, $P_a = 1$).

It is also interesting to observe the moderate effect of the limb darkening on such light curves of transiting exoplanets. Limb darkening is manifested mainly shortly before and after the transit and near the secondary eclipse. See Figure 6 with comments and description. It might be interesting to point out that extrasolar planets might show limb brightening at some wavelengths. This depends on the temperature gradient at a particular depth probed by a certain wavelength. If the temperature is decreasing one would observe limb darkening. If it is increasing one would observe limb brightening. There are two main effects which could cause a temperature inversion. (1) The presence of species high in the atmosphere effectively absorbing near the wavelength of maximum of the stellar energy redistribution. This would cause a temperature inversion, often called a stratosphere. (2) Heat redistribution between the day and the night side, especially if it occurs at deeper layers (Burrows et al. 2008). This might significantly cool such layers on the day side producing a drop in the temperature and an associated temperature inversion. This is the main motivation why we also study the effect of limb brightening in Figure 6 and its effect is just the opposite of limb darkening. It might be worth mentioning that all of the calculations mentioned above took into account the proper inclination of the orbit. Depending how close to edge-on the planet's orbit is, the observed light curve may vary by 5% simply due to the observer's viewing angle (Cowan & Agol 2008).

However, there are cases when the zonal temperature redistribution parameter, P_a, and limb darkening will be much more important. Figure 7 illustrates the situation for a hypothetical planet at an inclination of 20°. We used the parameters for the non-transiting close-in extrasolar planet HD179949b (Tinney et al. 2001; Cowan et al. 2007) to feed the code with real numbers. However, inclination, mass, and radius are not known for non-transiting exoplanets. In this case, the effects of the zonal temperature redistribution parameter and limb darkening are indeed important and are comparable to the amplitude of the light curve. Another point worth making is that there will be a strong degeneracy between the radius, P_r, and inclination since all of them affect the amplitude of the light curve. Also there may be a degeneracy between P_a, limb darkening, and radius, since all of them affect the mean level of the light curve. This justifies the complexity of our model with the heat redistribution and zonal temperature redistribution, and limb-darkening parameters. Gravity darkening is also included but this will not be an issue for the extrasolar planets. If they are close to the star then their intrinsic radiation is negligible compared to the heavy external irradiation and if they are far from the star then their shape will be almost spherical (neglecting the rotation) and without gravity darkening.

Finally, let us study how this Roche shape might affect the light curve of an extrasolar planet. This is illustrated in Figure 8 on the example of WASP-12b at 8 μm. The light varies by about 10% as predicted by Li et al. (2010). However, the

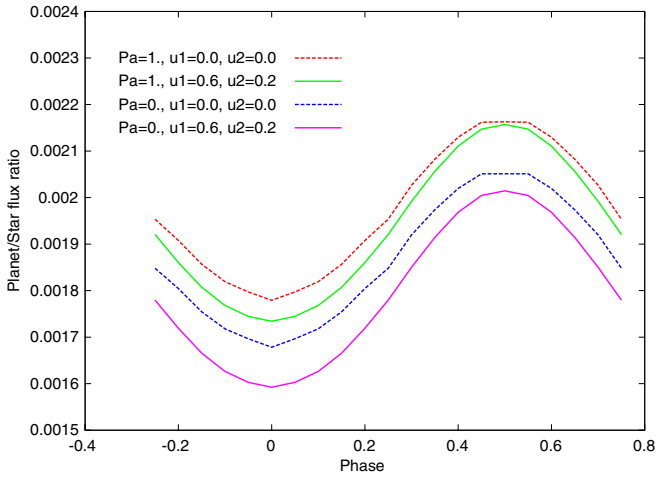

Figure 7. Effect of the zonal temperature redistribution (P_a parameter) and limb darkening on the light curve of a hypothetical exoplanet seen at a small inclination of 20°. Contrary to the case with homogeneous temperature distribution ($P_a = 1$), one would observe less flux from the models with the dominant east–west heat circulation ($P_a = 0$) since the polar regions visible at this inclination are quite cool. Limb darkening would dim the hotter equatorial regions even further and reduce the observed flux, especially for models with the dominant east–west heat circulation ($P_a = 0$). $A_B = 0$, $P_r = 0.5$ were assumed.

(A color version of this figure is available in the online journal.)

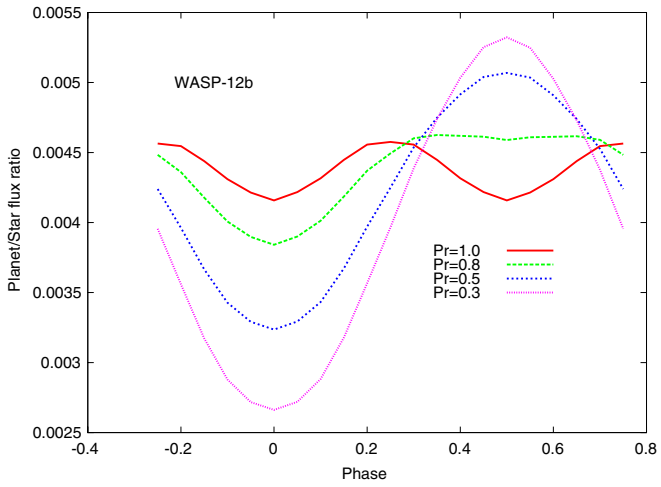

Figure 8. Illustration of the effect of the non-spherical shape on the light curve of WASP-12b at 8 μm. In the case of effective heat redistribution ($P_r = 1$), one would observe a highly atypical double-humped light curve caused by the Roche shape. This resembles the well-known ellipsoidal variations in interacting binaries. For lower values of P_r and less effective heat redistribution the light curve would acquire a more typical "cosine" shape. $A_B = 0$, $P_a = 1$, and zero limb darkening were assumed.

(A color version of this figure is available in the online journal.)

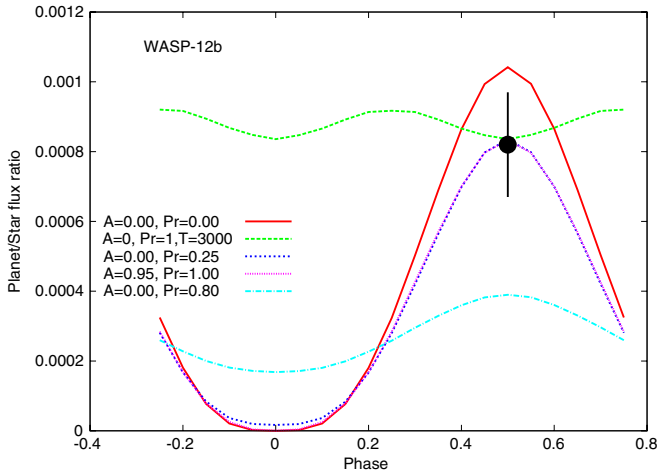

Figure 9. Light curves of WASP-12b at 0.9 μm. Observations of López-Morales et al. (2010), black point, can be understood within several very different models. A low albedo and low heat redistribution model ($A_B = 0$, $P_r = 0.25$) produces almost identical light curves compared with a high albedo model ($A_B = 0.95$, P_r is not very important in this case). Also a non-reflective model with homogeneous temperature distribution of about 3000 K ($A_B = 0$, $P_r = 1$, $P_a = 1$, $T_{\rm old} = 2600$ K) can reproduce the observations. Roche shape and zero limb darkening were assumed.

(A color version of this figure is available in the online journal.)

most striking thing is the double-humped light curve in the case of effective heat redistribution $P_r = 1$. This shape of the light curve gradually changes to a typical single-humped shape for less intense heat redistribution (lower values of P_r). The transition from double- to single-humped light curve is color dependent. Blackbody radiation at shorter wavelengths is more sensitive to the day–night temperature difference than radiation at longer wavelengths. Subsequently, the transition to a single-humped light curve occurs at higher P_r at shorter wavelengths. The truly double-humped light curve might be detected only for highly distorted planets with very intense and homogeneous heat redistribution at longer wavelengths. These calculations assumed the proper inclination of the orbit, zero albedo, zero limb darkening, and $P_a = 1$. Assuming $A_B = 0$, $P_r = 1$, $P_a = 1$, $T_{\rm old} = 100$ K, and Roche shape we obtained a mean temperature of the planet of 2470 K which is in good agreement with 2516 K obtained by Hebb et al. (2009) who assumed a spherical shape.

In the next step, we calculated the light curves of the planet at a much shorter wavelength (0.9 μm) and attempted to understand the secondary eclipse observations of López-Morales et al. (2010). This is illustrated in Figure 9. Note that at this shorter wavelength the light curves cover a considerable range of values during the secondary eclipse. This is in contrast to the longer wavelengths when light curves have a higher spread during the transit. This is also mainly because the blackbody radiation at shorter wavelengths is more sensitive to the day–night temperature difference than radiation at longer wavelengths. There is a lot of degeneracy between the albedo and heat redistribution in this case. For example, the observation of López-Morales et al. (2010) can be reproduced equally well by a model with $A_B = 0$, $P_r = 0.25$ with a mean surface temperature of 2470 K as well as by a model with $A_B = 0.95$, $P_r = 1$ with a mean surface temperature of 1170 K. Note that heat redistribution is not very important nor well constrained if the albedo is very high. It is also possible to fit the observations assuming that the surface is not reflective and the temperature is homogeneous over the entire surface ($A_B = 0$, $P_r = 1$, $P_a = 1$) and adopting $T_{\rm old} = 2600$ K. This corresponds to a mean temperature of the planet of about 3000 K (in this case the mean temperature is identical to the effective temperature and to the brightness temperature of the body). This is in agreement with a simple analytic model of Cowan & Agol (2010) and a blackbody brightness temperature of 3028 K estimated by López-Morales et al. (2010).

4.3. Spectra of the Close-in Extrasolar Planets

Calculations of the local atmosphere models and intensity emerging from the local atmosphere models on the surface of

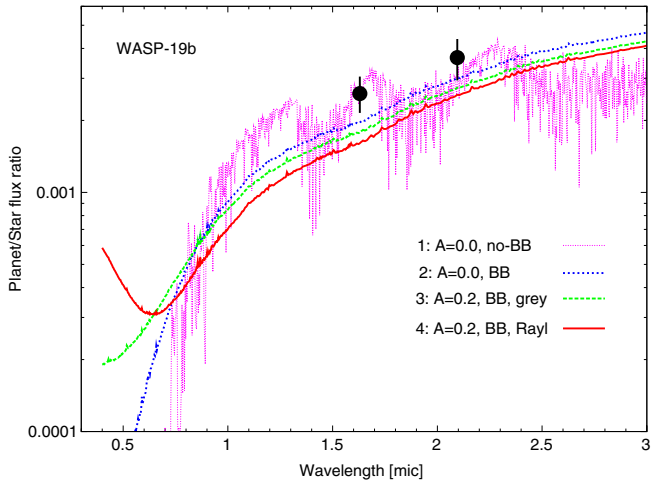

Figure 10. Planet-to-star flux ratio as a function of wavelength for WASP-19b. Model 2 is a blackbody model with zero albedo. Model 3 is a gray albedo model ($A_B = 0.2$). Model 4 is a non-gray albedo model (Rayleigh scattering) with the same Bond albedo, $A_B = 0.2$. Model 1 is a non-blackbody model based on non-irradiated atmospheres (Hubeny & Burrows 2007; Allard et al. 2003). Black symbols are measurements of Anderson et al. (2010b) and Gibson et al. (2010) in the *H* and *K* bands. Zero heat and homogeneous zonal temperature redistribution ($P_r = 0$, $P_a = 1$) and zero limb darkening were assumed.

(A color version of this figure is available in the online journal.)

the planet or star are beyond the scope of this paper. Grids of such models and spectra are available (Hubeny & Burrows 2007; Allard et al. 2003) which can be used as an input to our model. Subsequently, our code is not restricted to the blackbody approximation.

In this section, we apply our model to WASP-19b and study its spectrum. This planet was discovered by Hebb et al. (2010). The secondary eclipse was detected in the *H* band by Anderson et al. (2010b) and *K* band by Gibson et al. (2010). The authors found the emission from the planet very strong and it presents an interesting puzzle for the models. This is a highly distorted exoplanet and we assumed a proper shape according to the Roche potential, proper inclination, zero heat redistribution, homogeneous zonal temperature redistribution, zero limb and gravity darkening, and calculated spectra during the secondary eclipse. It was also assumed that the star has a spectrum given by Castelli & Kurucz (2004). As a first approximation for the planet I used the blackbody approximation. The comparison of the data with our model is in Figure 10. Our blackbody model with zero albedo and zero heat redistribution $P_r = 0$ still underpredicts the radiation from the planet but it is within 2σ from the measurements.

This figure also illustrates the effect of the albedo on the spectrum. For example, a relatively small frequency-independent (gray) albedo of about 0.2 will strongly increase the planet radiation at the shorter wavelengths but decrease the fluxes from the planet at wavelengths longer than 0.9 μm. This is because the non-zero albedo reduces the surface temperature of the planet but reflects the stellar light at shorter wavelengths. In the next step, we assumed that the albedo is not gray but has the following color dependence:

$$A_\nu = \frac{A_0(\lambda/\lambda_0)^\gamma}{(1-A_0)+A_0(\lambda/\lambda_0)^\gamma}, \qquad (35)$$

where A_0 is the albedo at some reference wavelength λ_0. We set $\gamma = -4$ to mimic the Rayleigh scattering with λ^{-4} dependence and adjust A_0 to recover the same Bond albedo (0.2) as in the previous case. This case produces identical surface temperatures as in the gray albedo case but radiation below 0.6 μm is considerably higher than in the gray case, radiation above the 0.6 μm is lower than in the gray case, and at still longer wavelength the relative difference between the gray and color albedo calculations gradually decreases. Finally, I refrained from the blackbody approximation for the planet and used the grid of non-irradiated atmosphere models of Hubeny & Burrows (2007) for $T_{\rm eff} < 1800$ K and Allard et al. (2003) (BT-Settl) for $T_{\rm eff} > 1800$ K. With this approach one can fit the observations of Anderson et al. (2010b) and Gibson et al. (2010) reasonably well. The fit requires that the planet has low Bond albedo and low heat redistribution. The stratosphere, if present, should not have a drastic impact on the spectrum since observations in both the *H* and *K* bands are above the blackbody curve. If the stratosphere were pronounced and *JHK* bands were reversed and were in absorption (instead of emission) it might be difficult to conserve the total flux and fit these observations simultaneously. Observations in the *J* and other bands would be extremely valuable.

5. CONCLUSIONS

I argue that the generally accepted reflection effect in interacting binaries must be revisited in order to properly describe the radiation from the cool object irradiated by the hot object. Subsequently, a new model for the reflection effect is proposed and applied to an extreme case of an interacting binary—an extrasolar planet plus star.

The new model introduces several free parameters. Some of them are well known in the field of extrasolar planets. (1) Bond albedo $A_B = \langle 0, 1\rangle$ which controls how much energy is reflected and how much is converted into heat. $A_B = 1$ means that all impinging energy is reflected off the surface and nothing is converted into heat. (2) Heat redistribution parameter $P_r = \langle 0, 1\rangle$ which controls how much heat from a certain point is redistributed to other places and how much is re-radiated locally. $P_r = 0$ means that all absorbed heat is re-radiated locally and nothing is transported to other locations. (3) Zonal temperature redistribution parameter $P_a = \langle 0, 1\rangle$ is a measure of the effectiveness of the homogeneous heat redistribution over the surface versus the zonal distribution. $P_a = 1$ means that the heat is homogeneously redistributed over the surface while $P_a = 0$ means zonal redistribution and that the heat flows only along the parallels. The model contains other parameters well known in the field of interacting binaries. (4) Fill-in parameter $f_i = \langle 0, 1\rangle$, and (5) mass ratio q which define the shape of the object. (6) Gravity darkening coefficient β which is usually set to 0.08 or 0.25 for convective and radiative envelopes, respectively. (7) Quadratic limb-darkening coefficients u_1, u_2. (8) Intrinsic surface temperature of the object in the absence of the irradiation $T_{\rm old}$ or T_p which is temperature at its rotation pole. There are other similar parameters which describe the second object: its radius, temperature, mass, rotation, movement, ...). Our model properly describes the shapes of the objects by means of the Roche potential and takes into account gravity and limb darkening. At the same time it takes into account the orbital revolution, rotation, and proper Doppler shifts in the scattered and thermal radiation. The code is freely available with the complete documentation and example runs at http://www.ta3.sk/~budaj/shellspec.html.

It is demonstrated on HD189733b that the light curves of transiting extrasolar planets are mainly sensitive to the heat redistribution parameter P_r and not so sensitive to the zonal temperature redistribution parameter P_a or to limb darkening.

However, light curves of planets seen at very low inclinations are also very sensitive to the zonal temperature redistribution parameter P_a as well as to limb darkening. This planet has a low Bond albedo and a relatively intense heat redistribution.

The effect of a non-spherical shape on the light curve can also be important. For highly distorted planets like WASP-12b this might cause a double-humped curve with an amplitude of about 10% superposed on other types of variability. Observations of this planet at 0.9 μm cannot constrain the Bond albedo or heat redistribution very well.

The effect of the gray and non-gray albedo on the spectrum of WASP-19b was also studied. It was demonstrated that a non-blackbody model with fluxes given by non-irradiated atmosphere models (Hubeny & Burrows 2007; Allard et al. 2003) can fit the observations of Anderson et al. (2010b) and Gibson et al. (2010) reasonably well. The planet has a low Bond albedo and a low heat redistribution.

We calculated the exact Roche shapes of all currently known transiting exoplanets (Schneider 1995) and found that the departures from spherical symmetry may vary significantly. Departures of the order of 1% are common, and can exceed about 8% in the most extreme cases like WASP-12b, WASP-19b, and WASP-33b. About 8% of transiting planets have departures more than 3% (all have semi-major axes smaller than 0.03 AU). The temperature redistribution over the surface of all these planets was also calculated. The mean temperatures of the planets vary considerably from 300 K to 2600 K. The extreme cases are WASP-33b, WASP-12b, and WASP-18b with mean temperatures of about 2600, 2430, and 2330 K, respectively.

I thank Professor Robert Wilson for a stimulating discussion, Dr. Nick Cowan, Professor Mercedes Richards, Professor Slavek Rucinski, and an anonymous referee for valuable comments on the manuscript, and Dr. Heather Knutson for sharing a copy of her data. The author acknowledges the support from the Marie Curie International Reintegration grant FP7-200297 and partial support from the VEGA grants 2/0078/10, 2/0074/09, 2/0094/11.

REFERENCES

Allard, F., Guillot, T., Ludwig, H.-G., Hauschildt, P. H., Schweitzer, A., Alexander, D. R., & Ferguson, J. W. 2003, in IAU Symp. 211, Brown Dwarfs, ed. E. Martín (San Francisco, CA: ASP), 325
Alonso, R., et al. 2004, ApJ, 613, L153
Alonso, R., et al. 2008, A&A, 482, L21
Anderson, D. R., et al. 2010a, ApJ, 709, 159
Anderson, D. R., et al. 2010b, A&A, 513, L3
Bakos, G., et al. 2007a, ApJ, 671, L173
Bakos, G., et al. 2007b, ApJ, 656, 552
Bakos, G., et al. 2009a, ApJ, 707, 446
Bakos, G., et al. 2009b, ApJ, 696, 1950
Bakos, G., et al. 2010, ApJ, 710, 1724
Baraffe, I., Chabrier, G., & Barman, T. 2008, A&A, 482, 315
Barge, P., et al. 2008, A&A, 482, L17
Barman, T. S., Hauschildt, P. H., & Allard, F. 2005, ApJ, 632, 1132
Barnes, J. W., & Fortney, J. J. 2003, ApJ, 588, 545
Bean, J. L., et al. 2008, A&A, 486, 1039
Borucki, W. J., et al. 2010a, ApJ, 713, L126
Borucki, W. J., et al. 2010b, Science, 327, 977
Bouchy, F., et al. 2005, A&A, 444, L15
Bouchy, F., et al. 2010, A&A, 519, 98
Bradstreet, D. H., & Steelman, D. P. 2002, BAAS, 34, 1224
Budaj, J., Burrows, A., Hubeny, I., & Ibgui, L. 2010, Highlights of Astronomy, 15, CD-ROM
Budaj, J., & Richards, M. T. 2004, Contrib. Astron. Obs. Skalnaté Pleso, 34, 167
Budaj, J., Richards, M. T., & Miller, B. 2005, ApJ, 623, 411
Burke, C., et al. 2007, ApJ, 671, 2115
Burke, C., et al. 2008, ApJ, 686, 1331
Burrows, A., Budaj, J., & Hubeny, I. 2008, ApJ, 678, 1436
Burrows, A., Hubeny, I., Budaj, J., & Hubbard, W. B. 2007, ApJ, 661, 502
Burrows, A., Sudarsky, D., & Hubeny, I. 2006, ApJ, 650, 1140
Carter, J.A, & Winn, J. N. 2010, ApJ, 709, 1219
Castelli, F., & Kurucz, R. L. 2004, arXiv:astro-ph/0405087
Charbonneau, D., et al. 2009, Nature, 462, 891
Claret, A. 1998, A&AS, 131, 395
Collier Cameron, A., et al. 2007, MNRAS, 380, 1230
Collier Cameron, A., et al. 2010, MNRAS, 407, 507
Cowan, N. B., & Agol, E. 2008, ApJ, 678, L129
Cowan, N. B., & Agol, E. 2010, arXiv:1001.0012
Cowan, N. B., Agol, E., & Charbonneau, D. 2007, MNRAS, 379, 641
Daemgen, S., Hormuth, F., Brandner, W., Bergfors, C., Janson, M., Hippler, S., & Henning, T. 2009, A&A, 498, 567
Deeg, H. J., et al. 2010, Nature, 464, 384
Deleuil, M., et al. 2008, A&A, 491, 889
Djurasevic, G. 1992, Ap&SS, 197, 17
Dobbs-Dixon, I., & Lin, D. N. C. 2008, ApJ, 673, 513
Drechsel, H., Haas, S., Lorenz, R., & Mayer, P. 1994, A&A, 284, 853
Dunham, E. W., et al. 2010, ApJ, 713, L136
Enoch, B., et al. 2010, MNRAS, in press (arXiv:1009.5917)
Fortney, J. J., Lodders, K., Marley, M. S., & Freedman, R. S. 2008, ApJ, 678, 1419
Fortney, J. J., Marley, M. S., & Barnes, J. W. 2007, ApJ, 659, 1661
Fossey, S. J., Waldmann, I. P., & Kipping, D. M. 2009, MNRAS, 396, L16
Fridlund, M., et al. 2010, A&A, 512, A14
Gibson, N. P., et al. 2008, A&A, 492, 603
Gibson, N. P., et al. 2010, MNRAS, 404, L114
Gillon, M., Pont, F., Moutou, C., Bouchy, F., Courbin, F., Sohy, S., & Magain, P. 2006, A&A, 459, 249
Gillon, M., et al. 2007, A&A, 466, 743
Gillon, M., et al. 2009, A&A, 501, 785
Guillot, T., Burrows, A., Hubbard, W. B., Lunine, J. I., & Saumon, D. 1996, ApJ, 459, L35
Guillot, T., & Showman, A. P. 2002, A&A, 385, 156
Hadrava, P. 1997, A&AS, 122, 581
Hansen, B. M. S. 2008, ApJS, 179, 484
Hartman, J. D., et al. 2009, ApJ, 706, 785
Hauschildt, P. H., Allard, F., & Baron, E. 1999, ApJ, 512, 377
Hebb, L., et al. 2009, ApJ, 693, 1920
Hebb, L., et al. 2010, ApJ, 708, 224
Hellier, C., et al. 2009, ApJ, 690, L89
Hellier, C., et al. 2010, ApJ, 723, L60
Henry, G. W., Marcy, G. W., Butler, R. P., & Vogt, S. S. 2000, ApJ, 529, L41
Hill, G. 1979, Publ. Dom. Astrophys. Obs. Victoria, 15, 297
Hubeny, I., & Burrows, A. 2007, ApJ, 669, 1248
Hubeny, I., Burrows, A., & Sudarsky, D. 2003, ApJ, 594, 1011
Jenkins, J. M., et al. 2010, ApJ, 724, 1108
Johns-Krull, C., et al. 2008, ApJ, 677, 657
Johnson, J. A., Winn, J. N., Cabrera, N. E., & Carter, J. A. 2009, ApJ, 692, L100
Joshi, Y. C., et al. 2008, MNRAS, 392, 1532
Kallrath, J., Milone, E. F., Terrell, D., & Young, A. T. 1998, ApJ, 508, 308
Kipping, D. M., & Tinetti, G. 2010, MNRAS, 407, 2589
Knutson, H., et al. 2007, Nature, 447, 183
Kopal, Z. 1959, Close Binary Systems (London: Chapman & Hall)
Kovacs, G., et al. 2007, ApJ, 670, L41
Latham, D. W., et al. 2009, ApJ, 704, 1107
Latham, D. W., et al. 2010, ApJ, 713, L140
Leconte, J., Chabrier, G., Baraffe, I., & Levrard, B. 2010, A&A, 516, A64
L'eger, A., et al. 2009, A&A, 506, 287
Li, S-L, Miller, N., Lin, D. N. C., & Fortney, J. J. 2010, Nature, 463, 1054
Linnell, A. P., & Hubeny, I. 1996, ApJ, 471, 958
Lister, T. A., et al. 2009, ApJ, 703, 752
López-Morales, M., Coughlin, J., Sing, D., Burrows, A., Apai, D., Rogers, J. C., & Spiegel, D. S. 2010, ApJ, 716, L36
Lucy, L. B. 1967, Z. Astrophys., 65, 89
Lucy, L. B. 1968, ApJ, 153, 877
Madhusudhan, N., & Seager, S. 2009, ApJ, 707, 24
Maxted, P. F. L., et al. 2010, AJ, 140, 2007
McCullough, P. R., et al. 2006, ApJ, 648, 1228
McCullough, P. R., et al. 2008, arXiv:0805.2921
Menou, K., & Rauscher, E. 2009, ApJ, 700, 887
Mochnacki, S. W., & Doughty, N. A. 1972, MNRAS, 156, 51
Moutou, C., et al. 2008, A&A, 488, L47

Noyes, R. W., et al. 2008, ApJ, 673, L79
O'Donovan, F. T., et al. 2007, ApJ, 663, L37
Orosz, J. A., & Hauschildt, P. H. 2000, A&A, 364, 265
Pál, A., et al. 2010, MNRAS, 401, 2665
Pavlovski, K., Burki, G., & Mimica, P. 2006, A&A, 454, 855
Plavec, M., & Kratochvil, P. 1964, Bull. Astron. Inst. Czech., 15, 165
Pont, F., Bouchy, F., Queloz, D., Santos, N. C., Melo, C., Mayor, M., & Udry, S. 2004, A&A, 426, L15
Pont, F., et al. 2007, A&A, 465, 1069
Pont, F., et al. 2008, A&A, 487, 749
Popper, D. M., & Etzel, P. B. 1981, AJ, 86, 102
Pribulla, T. 2004, in ASP Conf. Ser. 318, Spectroscopically and Spatially Resolving the Components of Close Binary Stars, ed. R. W. Hilditch et al. (San Francisco, CA: ASP), 117
Prša, A., & Zwitter, T. 2005, ApJ, 628, 426
Rauer, H., et al. 2009, A&A, 506, 281
Rucinski, S. M. 1969, Acta Astron., 19, 245
Rucinski, S. M. 1970, Acta Astron., 20, 327
Rucinski, S. M. 1973a, Acta Astron., 23, 79
Rucinski, S. M. 1973b, Acta Astron., 23, 301
Sahu, K. C., et al. 2006, Nature, 443, 534
Sato, B., et al. 2005, ApJ, 633, 465
Schneider, J. 1995, The Extrasolar Planets Encyclopaedia, http://exoplanet.eu
Seager, S., & Hui, L. 2002, ApJ, 574, 1004
Seager, S., Whitney, B. A., & Sasselov, D. D. 2000, ApJ, 540, 504
Showman, A. P., Fortney, J. J., Lian, Y., Marley, M. S., Freedman, R. S., Knutson, H. A., & Charbonneau, D. 2009, ApJ, 699, 564
Shporer, A., et al. 2009, ApJ, 690, 1393
Skillen, I., et al. 2009, A&A, 502, 391
Smalley, B., et al. 2010, A&A, 520, A56
Smith, A. M. S., et al. 2009, MNRAS, 398, 1827
Southworth, J., et al. 2009a, ApJ, 707, 167
Southworth, J., et al. 2009b, MNRAS, 399, 287
Southworth, J., et al. 2009c, MNRAS, 396, 1023
Street, R., et al. 2010, ApJ, 720, 337
Sudarsky, D., Burrows, A., Hubeny, I., & Li, A. 2005, ApJ, 627, 520
Tamuz, O., Mazeh, T., & North, P. 2006, MNRAS, 367, 1521
Tassoul, J.-L., & Tassoul, M. 1992, ApJ, 395, 259
Tinney, C. G., Butler, R. P., Marcy, G. W., Jones, H. R. A., Penny, A. J., Vogt, S. S., Apps, K., & Henry, G. W. 2001, ApJ, 551, 507
Tkachenko, A., Lehmann, H., & Mkrtichian, D. 2010, AJ, 139, 1327
Torres, G., et al. 2007, ApJ, 666, L121
Torres, G., et al. 2010, ApJ, 715, 458
Udalski., A., et al. 2008, A&A, 482, 299
Vaz, L. P. R., & Norlund, A. 1985, A&A, 147, 281
von Zeipel, H. 1924, MNRAS, 84, 665
Weldrake, D. T. F., Bayliss, D. D. R., Sackett, P. D., Tingley, B. W., Gillon, M., & Setiawan, J. 2008, ApJ, 675, L37
Welsh, W. F., Orosz, J. A., Seager, S., Fortney, J. J., Jenkins, J., Rowe, J. F., Koch, D., & Borucki, W. J. 2010, ApJ, 713, L145
West, R. G., et al. 2009, AJ, 137, 4834
West, R., et al. 2010, ApJ, submitted
Wilson, R. E. 1990, ApJ, 356, 613
Wilson, R. E. 1994, PASP, 106, 921
Wilson, R. E., & Devinney, E. J. 1971, ApJ, 166, 605
Winn, J. N., et al. 2007, AJ, 133, 1828
Winn, J. N., et al. 2009, ApJ, 693, 794
Wood, D. B. 1971, AJ, 76, 701
Zahn, J.-P. 1977, A&A, 57, 383
Zhang, E.-H., Robinson, E. L., & Nather, R. E. 1986, ApJ, 305, 740